

Phase transition in bilayer quantum Hall system with opposite magnetic field

Ke Yang(杨珂)

Citation: Chin. Phys. B, 2023, 32 (**9**): 097303. DOI: 10.1088/1674-1056/ace61d
Journal homepage: http://cpb.iphy.ac.cn; http://iopscience.iop.org/cpb

What follows is a list of articles you may be interested in

Entanglement spectrum of non-Abelian anyons

Ying-Hai Wu(吴英海)
Chin. Phys. B, 2022, 31 (**3**): 037302. DOI: 10.1088/1674-1056/ac280d

Topology and ferroelectricity in group-V monolayers

Mutee Ur Rehman, Chenqiang Hua(华陈强), Yunhao Lu(陆赟豪)
Chin. Phys. B, 2020, 29 (**5**): 057304. DOI: 10.1088/1674-1056/ab81ff

Phase diagram characterized by transmission in a triangular quantum dot

Jin Huang(黄金), Wei-Zhong Wang(王为忠)
Chin. Phys. B, 2018, 27 (**11**): 117303. DOI: 10.1088/1674-1056/27/11/117303

Quantum oscillations and nontrivial transport in $(Bi_{0.92}In_{0.08})_2Se_3$

Minhao Zhang(张敏昊), Yan Li(李焱), Fengqi Song(宋凤麒), Xuefeng Wang(王学锋), Rong Zhang(张荣)
Chin. Phys. B, 2017, 26 (**12**): 127305. DOI: 10.1088/1674-1056/26/12/127305

Quantum spin Hall and quantum valley Hall effects in trilayer graphene and their topological structures

Majeed Ur Rehman, A A Abid
Chin. Phys. B, 2017, 26 (**12**): 127304. DOI: 10.1088/1674-1056/26/12/127304

RAPID COMMUNICATION

Phase transition in bilayer quantum Hall system with opposite magnetic field

Ke Yang(杨珂)[†]

Kavli Institute for Theoretical Sciences, University of Chinese Academy of Sciences, Beijing 100190, *China*

(Received 5 May 2023; revised manuscript received 10 July 2023; accepted manuscript online 11 July 2023)

We construct a mapped bilayer quantum Hall system to realize the proposal that two nearly flatbands have opposite Chern numbers. For the $C = \pm 1$ case, the two Landau levels of the bilayer experience opposite magnetic fields. We consider a mapped bilayer quantum Hall system at total filling $\nu_t = \frac{1}{2} + \frac{1}{2}$ where the intralayer interaction is repulsive and the interlayer interaction is attractive. We take exact diagonalization (ED) calculations on a torus to study the phase transition when the separation distance d/l_B is driven. The critical point at $d_c/l_B = 0.68$ is characterized by a collapse of degeneracy and a crossing of energy levels. In the region $d/l_B < d_c/l_B$, the states of each level are highly degenerate. The pair-correlation function indicates electrons with opposite pseudo-spins are strong correlated at $\boldsymbol{r} = 0$. We find an exciton stripe phase composed of bound pairs. The ferromagnetic ground state is destroyed by the strong effective attractive potential. An electron composite-Fermion (eCF) and a hole composite Fermion (hCF) are tightly bound. In the region $d/l_B > d_c/l_B$, a crossover from the $d \to d_c$ limit to the large d limit is observed. The electron and hole composite Fermion liquids (CFL) are realized by composite Fermions (CF) which attach opposite fluxes, respectively.

Keywords: fractional quantum Hall effect, bilayer quantum Hall system, opposite magnetic field, quantum phase transition

PACS: 73.43.–f, 73.43.Nq **DOI:** 10.1088/1674-1056/ace61d

1. Introduction

Since the discovery of the quantum Hall effect (QHE), the interesting phenomenon has attracted long-lasting theoretical and experimental interest from researchers.[1] The quantum Hall (QH) state introduced the concept of topological order. The quantization of the Hall conductance is considered equivalent to a topological invariant.[2] The topological phase can be applied to both insulators and superconductors when an energy gap is active between the ground state and the excited states. The topological invariant as a topological order characterizes the nature of the topological state.[3] A filled band is equivalent to a filled Landau level and the Hall conductance is equivalent to the Chern number of a band as a topological invariant.[4] Topological phase in topological insulators can be characterized by Chern numbers of bands, and correlated states can be as an analogy of fractional quantum Hall (FQH) states induced by strong interaction.[5,6] In this paper we address the system in terms of multi-component FQH states as a fractional-quantum-Hall-like (FQHL) system. FQH effect has been extensively studied and people have a good understanding of various FQH states. After realizing particular FQH states in mapped bilayer quantum Hall system, we use numerical results from exact diagonalization (ED) and theoretical tools for FQH to understand the topological phases of the FQHL system.

The bilayer quantum Hall system (BQHS) has served as a platform for the research of strongly correlated physical phenomena induced by Coulomb interactions under large magnetic fields.[7–9] A bilayer system is established by two parallel layers of two-dimensional electron gas (2DEG) separated by a distance d/l_B (measured in units of the magnetic length l_B). Various quantum Hall (QH) states could be realized by tuning system parameters such as the scales of Coulomb interaction, the tunneling interaction and the Zeeman energy.[10–16] Typically, varying the separation d/l_B will lead to competition between intralayer interaction and interlayer interaction. The interlayer Coulomb interactions introduce the interlayer coherence until the separation d goes large enough. Phase transitions are driven during the two coupled 2DEG going decouple.[7,17]

The phases can be described as an exciton condensate of paired particles.[7,8,17–19] The picture is under a Landau quantization: the energy of 2DEG is quantized as the Landau levels (LL) within a perpendicular magnetic field $\boldsymbol{B}$. The filling factor ν at the lowest Landau levels (LLL) is defined as the radio $\nu = N_e/N_s$, that N_e is the number of electrons and N_s is the number of magnetic flux quanta through the area. A pseudospin analogy[20] is usually introduced: the index of layer plays a role as spin. The upper layer is labeled as $\uparrow$ and the other is labeled as $\downarrow$. The BQHS is then defined as a two-component fractional quantum Hall system.[21] The excitons are usually interpreted as electron–hole pairs. Electrons of one layer are bound to holes of the other layer.

[†]Corresponding author. E-mail: yangke@ucas.ac.cn

© 2023 Chinese Physical Society and IOP Publishing Ltd

The phases described by excitons of a small-separated and balanced filling bilayer system at $\nu_t = 1$ display the quantum Hall effect (QHE).[8,22] A quantized plateau of Hall conductance can be observed and the charged excitations have an energy gap. When separation $d/l_B \to 0$, the BQHS is reduced to a two-component monolayer quantum Hall system whose ground state is well known as the Halperin (111) state.[23] As the layer separation is increased, the exciton superfluid (SF) will vanish at a large enough critical separation d/l_B. As a result of decoupled layers, the system enters a compressible phase that can be described as composite Fermi liquid (CFL).[24] The closing of charge gap and vanishing quantized plateau of Hall conductance indicate the disappearance of QHE. The phase transition from exciton SF to CFL has been widely studied theoretically and experimentally.[25–33]

FQHE was also observed at total filling $\nu_t = 1/2$ in quantum well systems.[10,12,13,15] The states could be realized in a mapped two-component BQHS.[12,15] In limits of the separation $d \to 0$ and $d \to \infty$, the ground states of bilayer could be viewed as CFL. In the intermediate regime, the quantized plateau of Hall conductance and energy gap can be observed.[12] The ground states without interlayer tunneling are confirmed as the Halperin (331) state by numerical evidences.[15,34,35] The paired state can be viewed as a pair of composite fermions. When the interlayer tunneling is nonzero, a new phase transition from Abelian Halperin (331) state to non-Abelian Moore–Read Pfaffian state has been observed.[36,37] With various tunable parameters, new phase transitions[38,39] have been realized and analogous multi-component quantum Hall states filled in interacting particles (Fermions or Bosons[40,41]) have been observed at $\nu_t = 2/3$[16] and $\nu_t = 1/4$.[11] Compared to the one-component FQH system, the extra degrees of freedom introduce more tunable parameters that may be the origin of exotic paired states.[21] Those fractionalized topological states observed in quantum well systems[10,12] and topological flat band models[4,5,42,43] can be mapped to be realized in the BQHS.

The BQHS has been a powerful platform to realize various FQH states.[44] Real spin and pseudospin lead to four component states in each LL. Multi-component states indicate a richer combination of filling factors. The interlayer interaction and the tunneling term are easily tunable to realize various interlayer coherent states. The BQHS is expected to provide richer and more exotic quantum phase diagrams. The BQHS can be artificially realized in the quantum well system and bilayer graphene system. Thanks to the development of technology, particles and holes can both be filled in each layer. More FQH states have been realized easily.[1,10,11,13,45–47]

The strongly correlated phases in the nearly flat band models have attracted lots of attention. These topological phases are characterized by a non-zero Chern number C of the topological flatband. Recently the moiré superlattices of two-dimensional materials are established as powerful platforms to realize the nearly flat band systems.[48] Superconducting states[49] and correlated insulating states[50] are observed in moiré superlattices of twisted bilayer graphene. In such systems, the Coulomb interaction is important and the valley can be viewed as a pseudo-spin, then strongly inter-valley correlations can drive phase transitions. Opposite Berry curvatures in two valleys were observed in super-lattices and then researchers proposed that bands in two valleys can have opposite Chern numbers.[48,51–53] These states are similar to states in Chern insulators.[48] The states with opposite Chern numbers in two bands can be viewed as particles in two LLs experiencing opposite magnetic fields while the real spin is frozen.[52,54] Then those FQHL states can be viewed as an analogy of the FQH states and then be realized in a particular BQHS.[55,56]

Motivated by the above considerations we prefer to use the BQHS as a powerful ideal model for realizing ideal proposals. We focus on the FQHL system with strong interaction. The topological phase transitions are numerically simulated by ED within a mapped BQHS. In this paper, we build a simplified model to study the phase transition of a FQHL system with Chern numbers $C = \pm 1$ in two flatbands. In the mapped BQHS, particles in the mapped LLL of the two layers experience opposite magnetic fields. We focus on a balanced filling factor $\nu_t = \frac{1}{2} + \frac{1}{2}$. No tunneling and the real spins are frozen. The separation distance d/l_B is tuned to drive the new phase transition. The opposite magnetic field proposal could be further analogized as a BQHS with attractive interlayer interaction and repulsive innerlayer interaction under uniform magnetic fields. We perform exact diagonalization on torus geometry for the mapped BQHS. The paper is organized as follows. In Section 2 we will introduce the Hamiltonian of the mapped bilayer model and details of mapping are shown. In Section 3 we show the results from ED studies on the torus. The energy spectrum and the pair-correlation function are shown. In Section 4 we understand the phase transition in an effective field theory. A summary is given in Section 5.

2. Models and methods

The perpendicular magnetic field affects the cyclotron motion of a charged particle. Consider electrons moving in a 2D plane that experience a uniform perpendicular magnetic field. The single-particle Hamiltonian is described as

$$H_0 = \frac{(\boldsymbol{p} + e\boldsymbol{A}^{\xi}(\boldsymbol{r}))^2}{2m}, \tag{1}$$

where we take Landau gauge with the $\boldsymbol{B}$ dependent vector potential $\boldsymbol{A}^{\xi}(\boldsymbol{r}) = -\xi B(0, x, 0)$. We define $\xi = \pm 1$ for $\boldsymbol{B}_z = \mp B$, respectively. The commutation relation of the effective mo-

mentum $\boldsymbol{\pi} = \boldsymbol{p} + e\boldsymbol{A}^{\xi}(r)$ is written as

$$[\pi_x, \pi_y] = -\mathrm{i}e\hbar(\partial_x A_y^{\xi} - \partial_y A_x^{\xi}) = \mathrm{i}\xi e\hbar B = \mathrm{i}\xi\frac{\hbar^2}{l_B^2}, \quad (2)$$

where $l_B = \sqrt{\hbar/eB}$ is the magnetic length. The Hamiltonian of Eq. (1) can be well known as $H_0 = \hbar\omega_{\mathrm{c}}(a^{\dagger}a + \frac{1}{2})$. The canonical commutators satisfy $[a, a^{\dagger}] = 1$ and $\omega_{\mathrm{c}} = eB/m$. According to the commutation relation by Eq. (2), the introduced ladder operators could be written as

$$\begin{aligned} a_{+1}^{\dagger} &= \frac{l_B}{\hbar\sqrt{2}}(\pi_y + \mathrm{i}\pi_x), \quad a_{-1}^{\dagger} = \frac{l_B}{\hbar\sqrt{2}}(\pi_y - \mathrm{i}\pi_x), \\ a_{+1} &= \frac{l_B}{\hbar\sqrt{2}}(\pi_y - \mathrm{i}\pi_x), \quad a_{-1} = \frac{l_B}{\hbar\sqrt{2}}(\pi_y + \mathrm{i}\pi_x), \end{aligned} \quad (3)$$

where $\xi = \pm 1$ is related to the magnetic flux. The Landau levels $E_n = (n + \frac{1}{2})\hbar\omega_{\mathrm{c}}$ are in terms of quantum numbers n, which are the eigenvalue of operator $a^{\dagger}a$. The introduced ladder operators must satisfy the commutation relation $[a, a^{\dagger}] = 1$ subject to the constraints of Eq. (2). According to Eq. (3), we get a relationship of $a_{+1}^{\dagger} = a_{-1}$. The relationship demonstrates that a magnetic flux flip is equal to a particle–hole transform of the ladder operators.

The Hilbert space is limited to the lowest Landau level ($n = 0$). A set of plane wavefunctions are useful in constructing the single-particle wavefunction. We set $l_B = 1$ for convenience. According to the conserved momentum in y direction, the conserved quantum number k is important. We get a solution of $H_0\psi(\boldsymbol{r}) = E\psi(\boldsymbol{r})$ as

$$\psi_{\xi,m}(\boldsymbol{r}) = \frac{1}{\sqrt{L_y\pi^{1/2}}}\mathrm{e}^{\mathrm{i}my}\mathrm{e}^{-(x+\xi m)^2/2}. \quad (4)$$

We take a transformation $k = \xi m$ to remake the relation in Eq. (4). We get the function

$$\psi_{\xi,k}(\boldsymbol{r}) = \frac{1}{\sqrt{L_y\pi^{1/2}}}\mathrm{e}^{\mathrm{i}\xi ky}\mathrm{e}^{-(x+k)^2/2}. \quad (5)$$

Here $x = -k$ is the guiding center coordinate where the electrons are located at. The label ξ is defined in the y direction, with useful relation $\psi_{\xi,k} = \psi^*_{-\xi,k}$. This wavefunction describes a plane wave propagating in y with momentum $\xi\hbar k$.

To construct many-particle states we take the torus geometry where $L_x \times L_y = 2\pi N_{\mathrm{s}}$. N_{s} is the total magnetic flux towards the unit area and the orbital number $k = \frac{2\pi}{L_y}n_k$ with $n_k = 0, 1, \ldots, N_{\mathrm{s}} - 1$ according to the periodical boundary conditions. The wavefunctions described in Eq. (5) could be considered as single-particle wavefunctions located at site k. To create a particle at position $\boldsymbol{r}$, we use the fermionic field operators

$$\Psi_{\xi,\sigma}^{\dagger}(\boldsymbol{r}) = \sum_k \psi_{\xi,k}^*(\boldsymbol{r})c_{\xi,k,\sigma}^{\dagger}, \ \Psi_{\xi,\sigma}(\boldsymbol{r}) = \sum_k \psi_{\xi,k}(\boldsymbol{r})c_{\xi,k,\sigma}, \quad (6)$$

where the fermion operators $c_{\xi,k,\sigma}^{\dagger}, c_{\xi,k,\sigma}$ are defined in LLL of orbital k with spin σ under flux index ξ. These operators satisfy the canonical anti-commutation relations

$$\{c_{\xi k\sigma}^{\dagger}, c_{\xi' k'\sigma'}\} = \delta_{\xi,\xi'}\delta_{k,k'}\delta_{\sigma,\sigma'}. \quad (7)$$

Because the effect of magnetic flux flip is equal to the effect of a particle–hole transform, we have $c_{\xi}^{\dagger} = c_{-\xi}$. The many body states could be obtained by $|n_1 n_2 \cdots n_{N_{\mathrm{s}}}\rangle = \Pi_i^{N_{\mathrm{e}}} c_{\xi_i,k_i,\sigma_i}^{\dagger}|0\rangle$.

The density operator is defined as

$$\begin{aligned} \hat{\rho}_{\xi,\sigma}(\boldsymbol{q}) &= \int \mathrm{d}^2 r \mathrm{e}^{-\mathrm{i}\boldsymbol{q}\cdot\boldsymbol{r}}\Psi_{\xi,\sigma}^{\dagger}(\boldsymbol{r})\Psi_{\xi,\sigma}(\boldsymbol{r}) \\ &= \sum_{n_{k_1},n_{k_2}} \delta'_{n_{k_2}-n_{k_1},\xi n_{q_y}} \mathrm{e}^{\frac{\mathrm{i}\pi n_{q_x}(n_{k_1}+n_{k_2})}{N_{\mathrm{s}}}} \\ &\quad \times \mathrm{e}^{-\frac{q^2}{4}} c_{\xi,n_{k_1}}^{\dagger} c_{\xi,n_{k_2}}, \end{aligned} \quad (8)$$

where we define $q_i = \frac{2\pi}{L_i}n_{q_i}$ and δ' is the Kronecker delta defined modulo N_{s}. If we take $c_{\xi}^{\dagger} = c_{-\xi}$ in the representation, we then get

$$\hat{\rho}_{\xi,\sigma}(\boldsymbol{q}) \to -\hat{\rho}_{-\xi,\sigma}(\boldsymbol{q}). \quad (9)$$

The part of the constant energy will be discarded. From the above derivation, we find that ξ could also be considered as the charge of particles. The transform from '+' flux to '−' flux is equivalent to a particle–hole transform. When considering the two-body interactions, the differences between these two Hamiltonians will be discussed in Appendix B.

Consider the Coulomb interaction between particles. The total Hamiltonian is $H = H_{\mathrm{T}} + H_{\mathrm{int}}$, where the kinetic term H_{T} is constant that will be omitted due to strong interaction. According to the pseudospin analogy, $\uparrow$ labels one layer and $\downarrow$ labels the other. Electrons are filled in each layer, we have $\nu = \nu_{\uparrow} + \nu_{\downarrow}$. For convenience, we set $\xi = 1$ when $\sigma = \uparrow$ and $\xi = -1$ when $\sigma = \downarrow$. The index ξ is related to σ. The two-body Coulomb interaction Hamiltonian H_{int} is defined as

$$\begin{aligned} H_{\mathrm{int}} &= \frac{1}{2S}\sum_{\sigma,\sigma'} H_{\mathrm{int}}^{\sigma\sigma'}, \\ H_{\mathrm{int}}^{\sigma\sigma'} &= \sum_{\boldsymbol{q}} V_{\sigma\sigma'}(\boldsymbol{q})\rho_{\xi_{\sigma},\sigma}(-\boldsymbol{q})\rho_{\xi_{\sigma'},\sigma'}(\boldsymbol{q}). \end{aligned} \quad (10)$$

For the intralayer terms, we have $\sigma = \sigma'$. Drop the ξ index and the Hamitonian is simplified as $H_{\mathrm{int}}^{\sigma\sigma} = \sum_{\boldsymbol{q}} V_{\sigma\sigma}(\boldsymbol{q})\rho_{\sigma}(-\boldsymbol{q})\rho_{\sigma}(\boldsymbol{q})$. For the interlayer terms we have $\sigma \neq \sigma'$. According to Eq. (9), the interlayer term is simplified as

$$\begin{aligned} H_{\mathrm{int}}^{\sigma\sigma'} &= \sum_{\boldsymbol{q}} V_{\sigma\sigma'}(\boldsymbol{q})\rho_{\xi,\sigma}(-\boldsymbol{q})\rho_{-\xi,\sigma'}(\boldsymbol{q}) \\ &= \sum_{\boldsymbol{q}} -V_{\sigma\sigma'}(\boldsymbol{q})\rho_{\xi,\sigma}(-\boldsymbol{q})\rho_{\xi,\sigma'}(\boldsymbol{q}) \\ &= \sum_{\boldsymbol{q}} -V_{\sigma\sigma'}(\boldsymbol{q})\rho_{\sigma}(-\boldsymbol{q})\rho_{\sigma'}(\boldsymbol{q}). \end{aligned} \quad (11)$$

In the above equations we have transformed the density operator so that the two particles are under uniform magnetic field. The only effect is a negative sign which could be combined into electronic potential term $V_{\sigma\sigma'}(q)$. The repulsive interaction between electrons in different layers under opposite magnetic fields is equal to the attractive interaction between electrons in different layers under uniform magnetic fields. A mapped two-body Coulomb interaction Hamiltonian is written as

$$H_{\rm int} = \frac{1}{2S}\sum_{n_{k_1},n_{k_2},n_{k_3},n_{k_4}}\sum_{\sigma_1,\sigma_2} c^{\dagger}_{n_{k_1},\sigma_1}c^{\dagger}_{n_{k_2},\sigma_2}c_{n_{k_3},\sigma_2}c_{n_{k_4},\sigma_1} \times V^{\sigma_1,\sigma_2}_{n_{k_1},n_{k_2},n_{k_3},n_{k_4}}(\boldsymbol{q}), \tag{12}$$

where

$$V^{\sigma_1,\sigma_2}_{n_{k_1},n_{k_2},n_{k_3},n_{k_4}}(\boldsymbol{q}) = \sum_{\boldsymbol{q}\neq 0} V_{\sigma_1,\sigma_2}(\boldsymbol{q})\delta_{n_{k_1}-n_{k_4},n_{q_y}}\delta_{n_{k_2}-n_{k_3},-n_{q_y}} \times \mathrm{e}^{-\frac{|\boldsymbol{q}|^2}{2}}\mathrm{e}^{-\mathrm{i}\frac{2\pi n_{qx}}{N_{\rm s}}(n_{k_1}-n_{k_3})}. \tag{13}$$

The Coulomb interactions $V_{\sigma\sigma'}(\boldsymbol{q})$ are defined as $V_{\uparrow\uparrow}(\boldsymbol{q}) = V_{\downarrow\downarrow}(\boldsymbol{q}) = \frac{e^2}{(\varepsilon q)}$ and $V_{\uparrow\downarrow}(\boldsymbol{q}) = V_{\downarrow\uparrow}(\boldsymbol{q}) = \frac{-e^2}{(\varepsilon q)}\mathrm{e}^{-qd}$ for intralayer and interlayer, respectively.

3. Numerical results

In this paper we have performed exact diagonalization (ED) calculations in a mapped quantum Hall bilayers system at $\nu = \frac{1}{2}+\frac{1}{2}$. In the mapped model, the intralayer interaction is repulsive and the interlayer interaction is attractive. We work on the torus and the ratio L_y/L_x is unit. For a clear discussion, we address the lowest energy level E_0 as ground state energy $E_{\rm g}$ and the n-th lowest energy level as E_n.

In Fig. 1 we show the low energy levels versus layer distance d/l_B. We characterize the critical point at $d_{\rm c}/l_B \sim 0.68$. When distance d/l_B increases across $d_{\rm c}/l_B$, we can observe a significant collapse of degeneracy and the energy levels crossing. The characteristics indicate a critical point. When distance d/l_B continues increasing, several low-energy excited states decay exponentially to the energy levels of the ground state.

In the region of $d/l_B < d_{\rm c}/l_B$, the states in each level are highly degenerate. In Fig. 3(a), we show the highly degenerate states at different k sectors of $d/l_B = 0$. The ground states for $N_{\rm e} = 18$ are 20-fold degenerate, as shown in Fig. 1(a). The degenerate states are at sector $k_x = 0$ or $k_y = 0$. The black circle in Fig. 3(a) shows the degeneracy for the first excited energy levels. The first excited states for $N_{\rm e} = 18$ are also 20-fold, which are at sector $k_x = 1$ or $k_y = 1$. According to symmetry, we focus on sector $k_i \in [0,\pi], (i = x,y)$. We summarize that the degeneracy of states is $(N_{\rm e}+2)$-fold. The details of highly degenerate states are slightly different for $N_{\rm e}/2 =$ odd/even. For $N_{\rm e}/2 =$ odd, the degenerate states are at sectors $k_x = 0$ and $k_y = 0$ while for $N_{\rm e}/2 =$ even the degenerate states are at sectors $k_x = \pi$ and $k_y = \pi$. We take the system for $N_{\rm e} = 16$ as an example. The numerical results are shown in Fig. 1(b).

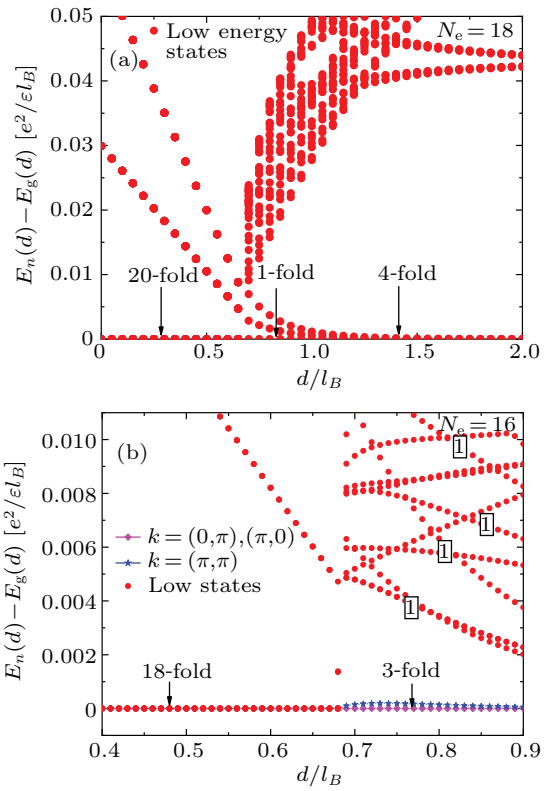


Fig. 1. The low energy levels as a function of layer separation d/l_B. We characterize $d_{\rm c}/l_B = 0.68$ as a critical point according to the collapse of degeneracy. We show the high degenerate states in each branch in $d/l_B < d_{\rm c}/l_B$. (a) The spectrum is for $N_{\rm e} = 18$. In the region $d < d_{\rm c}$, the states are 20-fold at ground states and the first excited states. The degeneracy is removed when d goes larger across $d_{\rm c}$. The lowest-energy state at $d/l_B \to d_{\rm c}/l_B$ limit is 1-fold. The three excited energy levels decrease to $\sim 10^{-4}$ with growing d/l_B. The lowest-energy states are 4-fold at large d limit. (b) The spectrum is for $N_{\rm e} = 16$. The states are 18-fold at ground states and the first excited states when $d < d_{\rm c}$. The lowest-energy state at $d/l_B \to d_{\rm c}/l_B$ limit seems 3-fold. There are numbers of extra energy levels that are exponentially decaying to the level of ground states with growing d/l_B. These levels are labeled by '1' in (b).

When increasing d/l_B passes through $d_{\rm c}/l_B$, the degenerate states in each level are removed. Energy level crossing is shown in Fig. 2(a). We show results of energy levels at various k sectors as a function of d/l_B. We plotted curves at the representative k sectors. The lowest energy level of $k = (\pi,\pi)$ remains at the energy-level scale of ground state. The ground energy level of $k = (0, 6\cdot\frac{2\pi}{N_{\rm s}})$ jumps from the energy level of ground state and continues increasing with increasing d/l_B. The ground energy level of $k = (0,\pi)$ jumps from the level of ground state and then continues decreasing exponentially to the level scale of ground state. The ground energy level of $k = (\pi,\pi)$ falls sharply and continues decreasing exponentially to the level scale of ground state too. The discontinuous curves of energy levels indicate a critical point. The first-order derivative curves of the ground-state energy as a function of

distance d/l_B are shown in Fig. 2(b). The curves for different system sizes exhibit a discontinuous behavior, which indicates a first order phase transition. The critical point can be confirmed at $d_c/l_B = 0.68$.

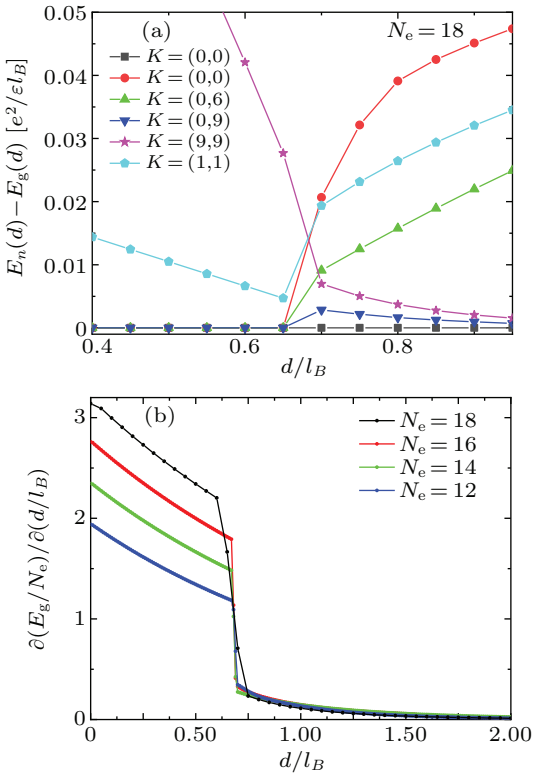


Fig. 2. Numerical evidence for the critical point. (a) The low energy levels of a function are plotted against layer separation d/l_B at different K sectors for $N_e = 18$. We show the energy level crossings between different K sectors at d_c/l_B. We set $k = K\frac{2\pi}{N_s}$. (b) The first-order derivative curves of the ground-state energy E_g/N_e as a function of layer separation d/l_B.

In Fig. 3 we study the energy gaps between the excited states and the ground states as a function of k. The blue line in Fig. 3(a) represents a nearly linear behavior. The energy levels of the selected points in the blue line are related to the energy levels of ground state at sector $k_y = k_x$. We measure the gaps between the excited states and ground states shown in Fig. 1(a) with the help of ground levels at $k_y = k_x$ sector shown in Fig. 3(a). The nearly linear relation is plotted in Fig. 3(c) as a function of $|k|$. The relation can be summarized as $\Delta E_n = E_g(k = (n,n)) - E_g \propto |k = (n,n)|$. ΔE_n is the gap between the n-th excited levels E_n and the ground levels E_g shown in Fig. 1(a). And $E_g(k)$ is the lowest energy level at k sector. As shown in Fig. 1(a), the gaps reduce with the increase of distance d/l_B in the region of $d < d_c$. We show the energy gaps as a function of $|k|$ at $d/l_B = 0.7$ in Fig. 3(b). As entering a new phase, the nearly linear relation is vanishing.

The system enters a new phase in the region of $d/l_B > d_c/l_B$. We divide the whole region into two limits. Depending on the scale of separation d/l_B, we address one as d_c limit and the other as large d limit. We argue if the states of the two limits are in one uniform phase.

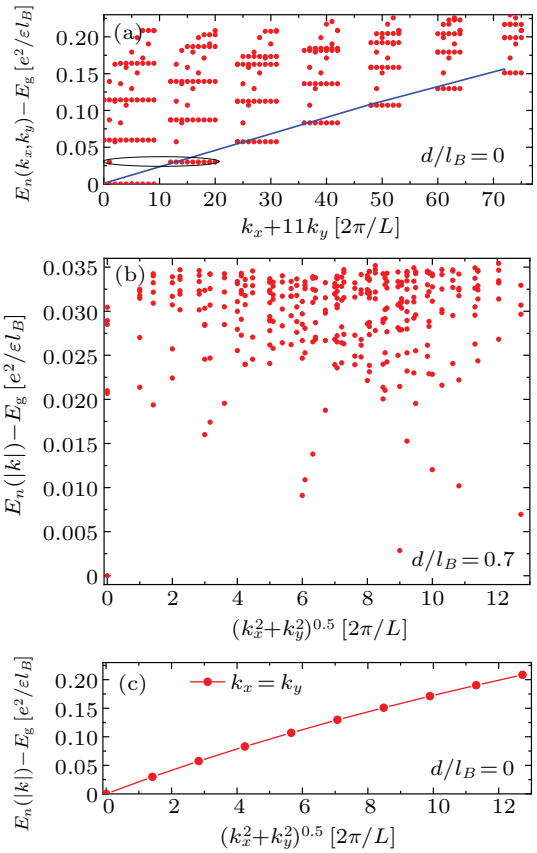


Fig. 3. Energy gaps as a function of k at $d/l_B = 0, 1.0$ for $N_e = 18$. (a) We show the energy gaps for $k = (k_x, k_y)$ at $d/l_B = 0$. $E_n(k_x,k_y) = E_n(k_y,k_x)$ is considered. The x-axis is defined as $k_x + 11k_y$. The blue line shows the nearly linear behavior of the levels of $k_x = k_y$ sector. The black circle shows the degenerate states in the first excited level. (b) We show the energy gaps as a function of $|k|$ at $d/l_B = 0.7$. (c) The nearly linear behavior of the ground levels as a function of $|k|$ at $k_x = k_y$ sector.

At the limit of $d/l_B \to d_c/l_B$, the state of the lowest level is at $k = (0,0)$ for $N_e = 18$ and $N_e = 14$. According to Fig. 1(a), we find the ground state of $k = (0,0)$ to be at the ground energy level. We address those as "fixed ground level". Three energy levels at sector $k = (0,\pi), (\pi,0)$ and (π,π) decay exponentially to the ground level as d/l_B increases when the degeneracy is removed, as shown in Fig. 2(a). We address those as "decreasing ground level". We also identify energy levels that increase with increasing d/l_B. Energy gaps of increasing states will reach a stable level at large d/l_B. We address those as "increasing excited level". The states of the fixed ground level should be described as 2-fold states at $k = (0,\pi), (\pi,0)$ for $N_e = 16$ and $N_e = 12$ in the region of intermediate d. The results for $N_e = 16$ shown in Fig. 1(b) raise an problem. For $d/l_B = 0.7 > d_c/l_B$ the gap is at scale of $\sim 10^{-4}$ between $E_g(k)$ of $k = (\pi,0)$, which is the ground state, and $E_g(k)$ of $k = (\pi,\pi)$ which is considered as a higher excited state. The gap energy level of ground state at $k = (\pi,\pi)$ exhibits an exponential decaying behavior versus increasing d/l_B, so we think that the ground state of $k = (\pi,\pi)$ should be referred to as "decreasing ground level". In Fig. 1(b), we find more exponential decaying energy levels with increasing d/l_B which are labeled as "1". They will keep decreasing to the ground level or the excited levels at large d limit. The high-energy levels that fall to ex-

cited levels at large d limit are summarized as "decreasing excited level". We have summarized the above behaviors in the region of intermediate d. The states of "fixed ground level" and "decreasing ground level" can be considered as ground states. When d/l_B is large enough, the energy levels of the corresponding states come to the scale of ground level. The same picture for $N_e = 16$ could be observed for $N_e < 18$. The extra decreasing levels that decrease to the ground level at large d are viewed as noises for $N_e < 18$. The picture for $N_e = 18$ is the ideal, as shown in Fig. 1(a). We speculate that the noises in the picture shown in Fig. 1(b) as an example come from the finite size effect. The summarized behaviors are valid for all the system sizes we used.

We consider the two layers to be completely decoupled at large d limit. The degeneracy of ground states increases with the low excited states decaying to the scale of ground states. In Fig. 4, we show the gaps $\Delta E(k_y)$ between the ground states of different k_y sectors at $d/l_B = 0.7$, 1.0 and 1.2 for $N_e = 18$. The falling of the ground energy level at $k_y = \pi$ could be observed. The energy dispersions settle into a mirror symmetrical structure at $d/l_B > 1$. The symmetric center is at $k_y = \pi/2$ and the relation could be expressed as $E_n(k_y) = E_n(\pi - k_y), (k_y \in [0, \pi])$. The similar results for $N_e = 16$ are shown in Fig. 5. At $d/l_B = 0.8$, the energy dispersions are complicated according to the energy spectrum shown in Fig. 1(b). As previously argued, the scales of these energy levels are close. It is difficult to determine a clear energy gap. We consider $E_g(k)$ of $k = (\pi, \pi)$ to be in the ground level. Compared to results in Fig. 4(a), the gap level $\Delta\tilde{E}$ of sector $k_y = \pi/2$ is at the same scale. At $d/l_B = 1.8$, the energy dispersions have a mirror symmetrical structure with the center at $k_y = \pi/2$. The decaying energy scale ~ 0.01 has been observed. We consider the states under the red dotted line as ground states. These levels are 'decreasing ground level'. The blue dashed line identifies the scale of gap above the ground states which continue growing slowly with increasing d/l_B. The mirror symmetrical structure and gap between 'decreasing ground level' and 'increasing excited level' are valid for $N_e = 12$ and $N_e = 14$.

We have reviewed features for d_c limit and the large d limit. There is no strong enough evidence to suggest that the two limits are in different phases. The summarized behaviors are applicable in the two limits. We observe a continuous transition. The crossover from the $d \to d_c$ limit to the large d limit is under uniform phase.

The Halperin (111) state can be described as the ferromagnetic ground state.[20] In the presence of Coulomb repulsion between the particles, each site is filled by a single electron on average. In Fig. 6 we show that the ferromagnetic ground state has been destroyed by the strong effective attractive potential. We define the following average occupancy: $\nu_d = \langle c^\dagger_{\uparrow,k} c^\dagger_{\downarrow,k} c_{\downarrow,k} c_{\uparrow,k} \rangle / N_e, \nu_{+1} = \langle c_{\downarrow,k} c^\dagger_{\downarrow,k} c^\dagger_{\uparrow,k} c_{\uparrow,k} \rangle / N_e, \nu_{-1} = \langle c_{\uparrow,k} c^\dagger_{\uparrow,k} c^\dagger_{\downarrow,k} c_{\downarrow,k} \rangle / N_e$. The definitions satisfy $\nu_{tot} = 2\nu_d + \nu_{-1} + \nu_{+1} = 1$. At $d/l_B \to 0$ we find the non-vanishing double occupied states in each k-sector of the degenerate ground states. Electrons with opposite spins are more likely to pair up.

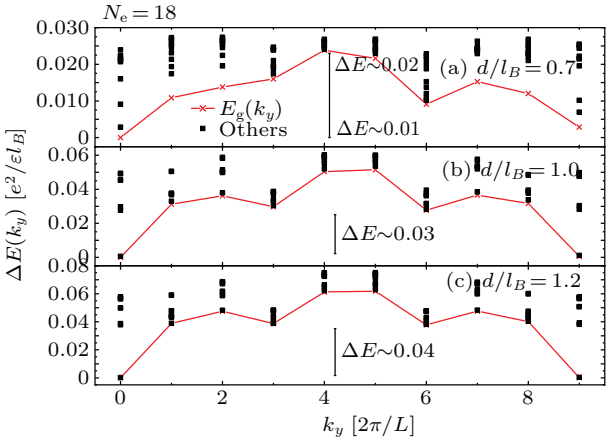


Fig. 4. The low energy levels as a function of k_y for $N_e = 18$ at $d/l_B = 0.7$, 1.0 and 1.2. The red crosses represent states of the lowest level at each k_y sector, and the black squares represent the states of the second lowest level at each k_y sector. The gap is considered as the difference between the lowest level and the next lower level. The energy scale of gap ΔE between the lowest excited states and the ground states is listed in each picture.

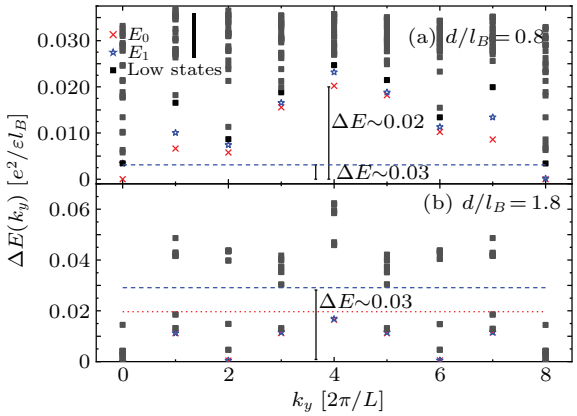


Fig. 5. The low energy levels as a function of k_y for $N_e = 16$ at $d/l_B = 0.8$, 1.8. The red crosses represent the lowest level of each k_y sector, the blue stars represent the second lowest levels and the black squares represent the other low levels at each k_y sector. We use blue dashed line to identify the scale of gap level. The states below the red dotted line are considered as degenerate ground states. The energy scale of gap between the lowest excited level and the ground level is listed in each picture.

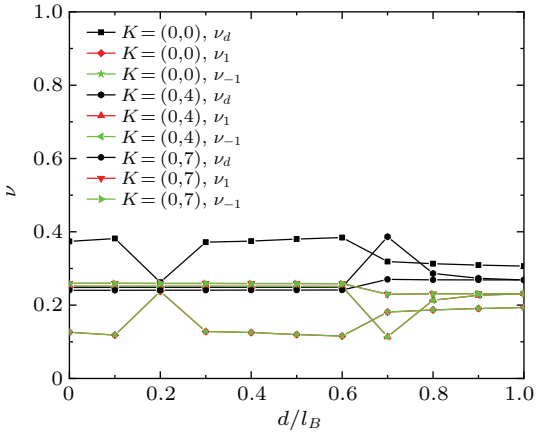


Fig. 6. Average occupancy per site at ground state as a function of separation d/l_B. The average occupancy at degenerate ground state is calculated for $N_e = 14$ at $K = (0,0), (0,4), (0,7)$ sectors. The results satisfy $2\nu_d + \nu_{-1} + \nu_{+1} = 1$.

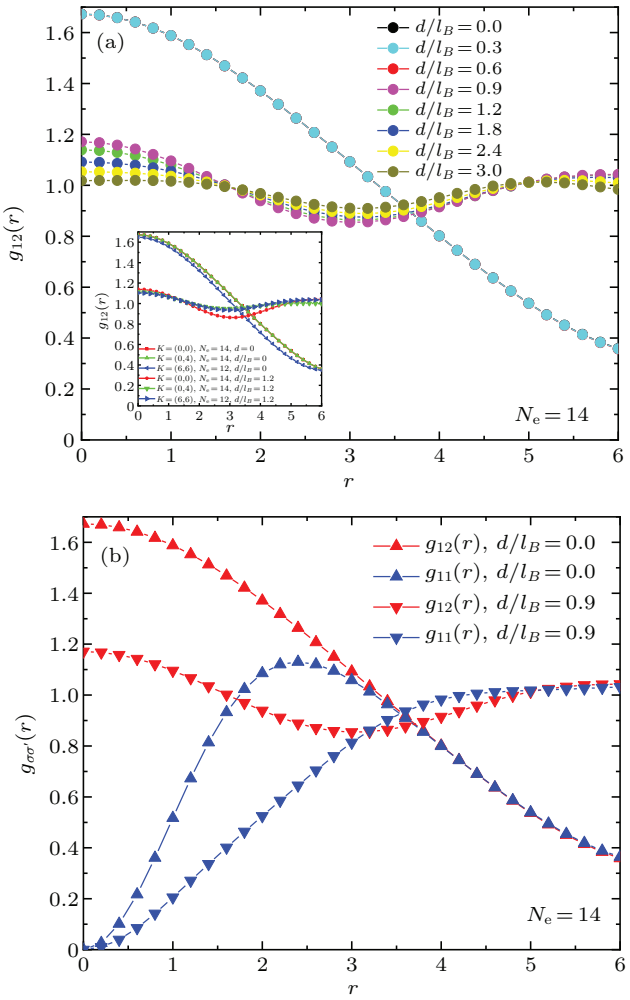


Fig. 7. The pair correlation function $g_{\sigma_1,\sigma_2}(\boldsymbol{r})$ at ground state for $N_e = 14$. We use $\boldsymbol{r} = (r/\sqrt{2}, r/\sqrt{2})$. (a) The interlayer pair correlation function $g_{12}(\boldsymbol{r})$ is shown as a function of separation d/l_B. The inner figure shows results in degenerate K-sector and results for $N_e = 12$. The results of main figure are calculated at $K = (0,0)$ sector. (b) We show the interlayer correlation function $g_{12}(\boldsymbol{r})$ and the intralayer $g_{11}(\boldsymbol{r})$ correlation function at $K = (0,0)$ sector. The separations are $d/l_B = 0.0 < d_c/l_B$ and $d/l_B = 0.9 > d_c/l_B$.

The exciton superfluidity is well understood as a Bose–Einstein condensation (BEC) of paired-state via a particle–hole transformation in single layer.[63] Each pair is viewed as a bound state of two particles, described by an exciton wave function.[28] In a similar picture, we check the two-particle correlations to determine the order of the ground state. The interlayer pair correlation function is defined as

$$g_{12}(\boldsymbol{r}) = \frac{1}{\nu_\uparrow \nu_\downarrow}\langle \Phi_\uparrow^\dagger(\boldsymbol{R_1})\Phi_\downarrow^\dagger(\boldsymbol{R_2})\Phi_\downarrow(\boldsymbol{R_2})\Phi_\uparrow(\boldsymbol{R_1})\rangle, \quad (14)$$

where Φ is the field operator and $\boldsymbol{r} = \boldsymbol{R_1} - \boldsymbol{R_2}$. The intralayer pair correlation function is similarly defined as $g_{11}(\boldsymbol{r}) = \frac{1}{\nu_\uparrow^2}\langle \Phi_\uparrow^\dagger(\boldsymbol{R_1})\Phi_\uparrow^\dagger(\boldsymbol{R_2})\Phi_\uparrow(\boldsymbol{R_2})\Phi_\uparrow(\boldsymbol{R_1})\rangle$. In $d/l_B < d_c/l_B$, we calculate $g_{12}(\boldsymbol{r})$ in each K-space at degenerate ground state. As illustrated in the inner figure of Fig. 7(a), we can obtain an equal value of $g_{12}(\boldsymbol{r})$ for each degenerate K-space. In comparison, the results of $d/l_B = 1.2$ show that lifting the degenerate ground state causes differences in the K-sector. We show the interlayer pair-correlation function at different d/l_B in the ground sector $K = (0,0)$ for $N_e = 14$ in Fig. 7(a) and the intralayer pair-correlation function at $d/l_B = 0, 0.9$ in Fig. 7(b). In the region $d/l_B < d_c/l_B$, the peak of $g_{12}(\boldsymbol{r})$ at $r = 0$ and the vanishing of $g_{11}(\boldsymbol{r} = 0)$ indicate an interlayer strongly correlated state. The intralayer pair-correlation function also has a peak at $r \sim 2.5$. The observed peaks show strong short-range correlation. The spin-↑ and spin-↓ are filled at the same location. An exciton crystal is characterized in the fields of electron–hole plasmas[57] and the interacting bosonic gas.[58,59] The curves of pair correlation remain unchanged as d/l_B varies. In the region $d/l_B > d_c/l_B$, $g_{12}(\boldsymbol{r})$ approaches 1 as d/l_B increases, and $g_{11}(\boldsymbol{r})$ grows from 0 to 1 with increasing $\boldsymbol{r}$. The features of pair-correlation function characterize a similar behavior described in the CFL limit.[64]

In Fig. 8, we calculate $g(\boldsymbol{r})$ in different r_x and r_y to clarify the spatial structure at the ground state. We find stripe correlations. The numerical studies for the stripe ground state at specific filling factor ν in the lowest Landau level have been well understood in Refs. [25,60]. The characteristics of the correlation function are consistent with the feature of the nearly degenerated ground state when $d/l_B < d_c/l_B$. A similar phase is obtained in the study of Ref. [61], where the negative interlayer attraction is strong enough. The ground state has been proposed as a charge density wave (CDW) order by Rezayi.[62] The wavelength of the stripe is related to L_y. The competition between attraction and repulsion drives the phase transition and the translational symmetry is breaking.

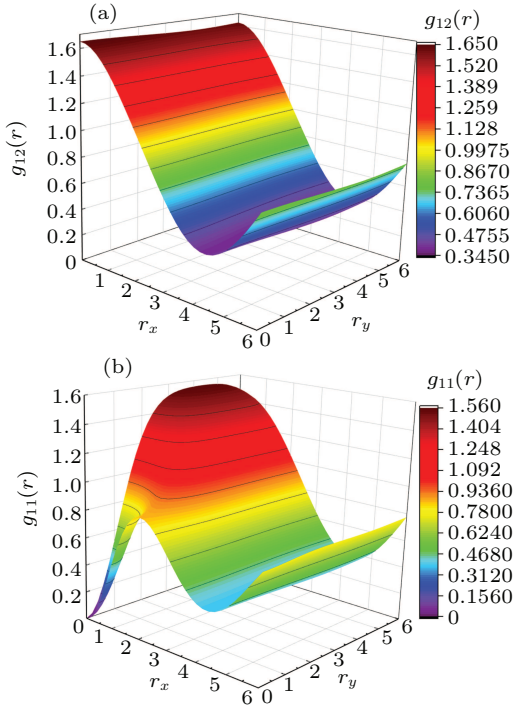


Fig. 8. The pair correlation function $g_{\sigma_1,\sigma_2}(\boldsymbol{r})$ at ground state for $N_e = 12$ in the region $d/l_B < d_c/l_B$. We observe a stripe ground state. (a) The interlayer correlation function $g_{12}(\boldsymbol{r})$. (b) The intralayer $g_{11}(\boldsymbol{r})$ correlation function.

4. Discussion

When we consider a system of Fermi gas, the interactions between fermions could be described via a potential $V(r)$. Early researches for superconductivity in heavy-fermion systems and superfluidity in liquid ^{3}He suggested the importance of an effective attractive potential.[65–67] The strong attractive coupling will drive pairs of fermions to be tightly bound.[67] The two-body tightly bound state can be described by composite bosons (CB). People have realized the pair states in ultracold atomic gases.[68,69] In ultracold atomic gases, the effective interaction potential can be tuned from negative value to positive value with Feshbach resonances related to a magnetic field.[70] In the strong attractive potential, strongly paired bosonic molecules condensation can be predicted.[71,72] The paired fermionic superfluid can be introduced to quantum Hall effect regimes with an effective field theory description.[72,72] In this section we will describe the phase transition based on the developed effective field theory.

The single $\nu = 1/2$ two-dimensional electron gases under magnetic field realize a composite Fermion liquid (CFL). Electrons attaching opposite flux quanta can be described as e-CF and h-CF, respectively. In the limit of $d/l_B \to \infty$, the electron and hole composite Fermion liquids are realized. People have proposed that eCF–hCF pairs drive bilayer quantum Hall system into a Bose–Einstein condensate phase as the interlayer interactions become strong enough.[28,63] In the limit of $d/l_B \to 0$, the attractive interlayer potential leads to bound states. The two limits can be considered as single fermionic atom limit and paired bosonic molecule limit. The composite boson carries two charges and two masses compared to a single fermion. We can have the constraints

$$N_{\rm e} = \sum_{\sigma} \langle N_\sigma \rangle + 2\langle N_{\rm b} \rangle, \tag{15}$$

where $N_{\rm e}$ is the total number of electrons. We introduce the field $\Phi^\dagger(\boldsymbol{r}-\boldsymbol{r}') = \psi_\uparrow^\dagger(\boldsymbol{r})\psi_\downarrow^\dagger(\boldsymbol{r}')$ as the pair bosonic field. Then we can write the effective lagrangian density as

$$\begin{aligned}
\mathcal{L} &= \sum_\sigma \mathcal{L}_\sigma + \mathcal{L}_{\rm B} + \mathcal{L}_{\rm CS} + g(\Phi^\dagger \psi_\uparrow \psi_\downarrow + \Phi \psi_\uparrow^\dagger \psi_\downarrow^\dagger), \\
\mathcal{L}_\sigma &= \psi_\sigma^\dagger (\mathrm{i}\partial_t - a_0^\sigma)\psi_\sigma - \mu_\sigma |\psi_\sigma|^2 \\
&\quad + \frac{1}{2m} |\left(-\mathrm{i}\nabla - (A^\sigma + a^\sigma)\right)\psi_\sigma|^2 + \cdots, \\
\mathcal{L}_{\rm B} &= \Phi^\dagger(\partial_t - a_0^\uparrow - a_0^\downarrow)\Phi - (\mu_\uparrow + \mu_\downarrow - \delta)|\Phi|^2 \\
&\quad + \frac{1}{2M}|(-\mathrm{i}\nabla - (\sum_\sigma A^\sigma + a^\sigma))\Phi|^2 + \cdots, \\
\mathcal{L}_{\rm CS} &= \mathcal{L}_{\rm CS}^\uparrow + \mathcal{L}_{\rm CS}^\downarrow \\
&= \frac{1}{4\pi}\frac{\pi}{\theta}\varepsilon^{\mu\nu\lambda}[a_\mu^\uparrow \partial_\nu a_\lambda^\uparrow + \xi a_\mu^\downarrow \partial_\nu a_\lambda^\downarrow].
\end{aligned} \tag{16}$$

The field ψ_σ describes the composite Fermion fields of spin-σ, and a^σ is the corresponding Chern–Simons (CS) gauge field. a^σ attaches θ/π flux which is related to ψ_σ. We set $\theta = 2\pi$ for $\nu_\sigma = 1/2$. When we consider an opposite magnetic field, we need $A^\uparrow = -A^\downarrow$ in average and set $\xi = -1$ to indicate the opposite directions for different spins.[73] The $\mathcal{L}_{\rm B}$ describes the pair fields. Here the parameter δ is always used in tuning the repulsive and attractive interaction in ultra cold gas.[72] The CF field in each layer is coupled to pair field Φ via the g term in $\mathcal{L}$. Generally, people use a mean field treatment as $h = g\langle\Phi(r)\rangle$ to estimate the phase diagram. If $\langle\Phi(r)\rangle \neq 0$, we can claim that there exist the composite bosons. The CB sees no external field A and carries double charges. The peaked curves of $g_{12}(\boldsymbol{r})$ at $\boldsymbol{r} = 0$ suggest the existence of bound state. The existence of superfluidity is denied by the peaked curves of $g_{11}(\boldsymbol{r})$ at small $\boldsymbol{r}$. The results in Fig. 8 indicate that a stripe state is formed. When $\langle\Phi(r)\rangle$ vanishes, we claim that the two CF fields construct CFL respectively with effective opposite charge which attach 2 units of flux. The introduced field consists of CFs as $\psi_\uparrow\psi_\downarrow$, which drives a first order phase transition from an exciton stripe phase composed of eCF–hCF bound pairs to an eCFL–hCFL phase.

5. Conclusion

By analyzing the energy spectrum, we characterize a critical point at $d_{\rm c}/l_B = 0.68$. When separation d increases across $d_{\rm c}$, a significant collapse of degeneracy, energy levels crossing and discontinuous first-order derivative curves of the ground-state energy could be observed. In the region $d < d_{\rm c}$, the states in each level are highly degenerate, and the the degeneracy is a signal of the spontaneous breaking of translational symmetry.[61] In the region $d > d_{\rm c}$, the high degeneracy is removed. The system goes through a crossover from the $d \to d_{\rm c}$ limit to the large d limit.

The pair-correlation function $g_{12}(\boldsymbol{r})$ shows the evidence of strong bound pair at $\boldsymbol{r} = 0$. When $d/l_B < d_{\rm c}/l_B$, the strong effective attractive potential makes it easier to bind electrons with opposite spins. The ferromagnetic ground state is destroyed. The peak of $g_{12}(\boldsymbol{r})$ at $r = 0$ and $g_{11}(\boldsymbol{r})$ at $r \sim 2.5$ indicate an exciton stripe state. As d/l_B grows through $d_{\rm c}/l_B$, the behavior of pair correlation functions indicates an eCFL–hCFL phase. We follow the effective field theory developed by Yang[72] to understand the phase transition. CF is constructed by electron attaching two fluxes. Opposite flux leads to opposite effective charge. The competition between the interlayer interaction and the intralayer interaction drives the phase transition. When $d/l_B < d_{\rm c}/l_B$, the effective attractive interlayer interaction drives the eCF to bind with hCF. The composite Bosons with effective repulsive potential form the stripe states. When the two layers are decoupled, the bound state is destroyed. CFs form CFL with opposite effective charges in each layer.

Appendix A: The density operator

Here we show the derivation details of the density operator when a flux index is considered. The $\rho_{\xi,\sigma}(r)$ is defined as

$$\begin{aligned}
\hat{\rho}_{\xi,\sigma}(q) &= \int \mathrm{d}^2 r \mathrm{e}^{-\mathrm{i}\boldsymbol{q}\cdot\boldsymbol{r}} \Psi^{\dagger}_{\xi,\sigma}(\boldsymbol{r}) \Psi_{\xi,\sigma}(\boldsymbol{r}) \\
&= \frac{1}{L_y\sqrt{\pi}} \sum_{k_1,k_2} c^{\dagger}_{\xi,k_1} c_{\xi,k_2} \int \mathrm{d}x\mathrm{d}y \mathrm{e}^{\mathrm{i}\xi y(k_2-k_1)-\mathrm{i}(q_x x+q_y y)} \mathrm{e}^{-[(x+k_1)^2+(x+k_2)^2]/2} \\
&= \frac{1}{\sqrt{\pi}} \sum_{k_1,k_2} c^{\dagger}_{\xi,k_1} c_{\xi,k_2} \delta'_{k_2-k_1,\xi q_y} \int \mathrm{d}x \mathrm{e}^{-\mathrm{i}q_x(x-(k_1+k_2)/2)} \mathrm{e}^{-(x+\xi q_y)^2/2-(x-\xi q_y)^2/2} \\
&= \frac{1}{\sqrt{\pi}} \sum_{k_1,k_2} c^{\dagger}_{\xi,k_1} c_{\xi,k_2} \delta'_{k_2-k_1,\xi q_y} \mathrm{e}^{\mathrm{i}q_x(k_1+k_2)/2} \mathrm{e}^{-\frac{1}{4}(q_x^2+q_y^2)} \int \mathrm{d}x \mathrm{e}^{-(x^2+\mathrm{i}q_x x-q_x^2/4)} \\
&= \sum_{k_1,k_2} c^{\dagger}_{\xi,k_1} c_{\xi,k_2} \delta'_{k_2-k_1,\xi q_y} \mathrm{e}^{\mathrm{i}q_x(k_1+k_2)/2} \mathrm{e}^{-\frac{1}{4}q^2} \\
&= \sum_{n_{k_1},n_{k_2}} c^{\dagger}_{\xi,n_{k_1}} c_{\xi,n_{k_2}} \delta'_{n_{k_2}-n_{k_1},\xi n_{q_y}} \mathrm{e}^{\mathrm{i}\frac{2\pi n_{q_x}}{N_s}(n_{k_1}+n_{k_2})/2} \mathrm{e}^{-\frac{1}{4}q^2}.
\end{aligned} \tag{A1}$$

Define the matrix elements as $M(q_x,k_1,k_2) = \exp(\mathrm{i}\frac{2\pi n_{q_x}}{N_s}\frac{n_{k_1}+n_{k_2}}{2})\exp(-\frac{q^2}{4})$ for convenience. Easy to know $M(q_x,k_1,k_2) = M(q_x,k_2,k_1)$. Take a transform $c^{\dagger}_{\xi} = c_{-\xi}$ then we will have

$$\begin{aligned}
\hat{\rho}_{\xi,\sigma}(q) &= \sum_{n_{k_1},n_{k_2}} \delta'_{n_{k_2}-n_{k_1},\xi n_{q_y}} M(q_x,k_1,k_2) c^{\dagger}_{\xi,n_{k_1}} c_{\xi,n_{k_2}} \to -\sum_{n_{k_1},n_{k_2}} \delta'_{n_{k_1}-n_{k_2},-\xi n_{q_y}} M(q_x,k_2,k_1) c_{\xi,n_{k_2}} c^{\dagger}_{\xi,n_{k_1}} \\
&= \sum_{n_{k_2},n_{k_1}} \delta'_{n_{k_2}-n_{k_1},-\xi n_{q_y}} M(q_x,k_1,k_2) c^{\dagger}_{-\xi,n_{k_1}} c_{-\xi,n_{k_2}} = \hat{\rho}_{-\xi,\sigma}(q).
\end{aligned} \tag{A2}$$

This relation could similar be got via $\hat{\rho}(\boldsymbol{q}) = \frac{1}{V}\sum_{\boldsymbol{q}} \mathrm{e}^{\mathrm{i}\boldsymbol{q}\boldsymbol{r}}\hat{\rho}(\boldsymbol{r})$ where

$$\hat{\rho}_{\xi,\sigma}(\boldsymbol{r}) = \sum_{k_1 k_2} \psi^{*}_{\xi,k_1}(\boldsymbol{r}) \psi_{\xi,k_2}(\boldsymbol{r}) c^{\dagger}_{\xi,k_1} c_{\xi,k_2} \to -\sum_{k_1,k_2} \psi^{*}_{-\xi,k_1}(\boldsymbol{r}) \psi_{-\xi,k_2}(\boldsymbol{r}) c^{\dagger}_{-\xi,k_1} c_{-\xi,k_2} = -\hat{\rho}_{-\xi,\sigma}(\boldsymbol{r}). \tag{A3}$$

Appendix B: Particle–hole transform and opposite fluxes

Interaction potential could be defined as $V_{\mathrm{ee}}(q) = -V_{\mathrm{eh}}(q)$, where 'ee' is for electron–electron interaction and 'eh' is for electron–hole interaction, respectively.

In the main paper, we have discussed the relations of the density operator under the index of flux and under particle–hole transformation. We omit the spin-index and use e for electron, h for hole and $\pm$ for flux. We define the classical two-body electron–electron interaction Hamitonian as $H_{\mathrm{ee}} = \sum_q V_{\mathrm{ee}}\rho_{\mathrm{e}+}(-q)\rho_{\mathrm{e}+}(q)$. For flux flip and particle–hole transform, we easily have

$$\rho_{-} = -\rho_{+}, \quad \rho_{\mathrm{e}} = -\rho_{\mathrm{h}}. \tag{B1}$$

Then we define the electron–hole interaction Hamitonian under uniform flux H_{eh} and the electron–electron interaction Hamitonian under opposite flux H_{+-}

$$\begin{aligned}
H_{\mathrm{eh}} &= \sum_q V_{\mathrm{eh}}\rho_{\mathrm{h}+}(-q)\rho_{\mathrm{e}+}(q) \\
&= \sum_q V_{\mathrm{ee}}\rho_{\mathrm{e}+}(-q)\rho_{\mathrm{e}+}(q) = H_{\mathrm{ee}}, \\
H_{+-} &= \sum_q V_{\mathrm{ee}}\rho_{\mathrm{e}-}(-q)\rho_{\mathrm{e}+}(q) \\
&= \sum_q -V_{\mathrm{ee}}\rho_{\mathrm{e}+}(-q)\rho_{\mathrm{e}+}(q) = -H_{\mathrm{ee}}.
\end{aligned} \tag{B2}$$

Acknowledgement

We would like to thank Zhu Zheng for discussions.

References

[1] Halperin B I and Jain J K 2020 *Fractional quantum hall effects: new developments*, 1st Ed. (World Scientific)
[2] Niu Q, Thouless D J and Wu Y S 1985 *Phys. Rev. B* **31** 3372
[3] Wen X G 1995 *Adv. in Phys.* **44** 405
[4] Parameswaran S A, Roy R and Sondhi S L 2013 *Com. Ren. Phys.* **14** 816
[5] Neupert T, Santos L, Chamon C and Mudry C 2011 *Phys. Rev. Lett.* **106** 236804
[6] Levin M and Stern A 2009 *Phys. Rev. Lett.* **103** 196803
[7] Eisenstein J P 2014 *Annu. Rev. Condens. Matter Phys.* **5** 159
[8] Eisenstein J P and MacDonald A H 2004 *Nature* **432** 691
[9] Barkeshli M and Wen X G 2011 *Phys. Rev. B* **84** 115121
[10] Suen Y W, Engel L W, Santos M B, Shayegan M and Tsui D C 1992 *Phys. Rev. Lett.* **68** 1376
[11] Luhman D R, Pan W, Tsui D C, Pfeiffer L N, Baldwin K W and West K W 2008 *Phys. Rev. Lett.* **101** 266804
[12] Shabani J, Liu Y, Shayegan M, Pfeiffer L N, West K W and Baldwin K W 2013 *Phys. Rev. B* **88** 245413
[13] Liu Y, Graninger A L, Hasdemir S, Shayegan M, Pfeiffer L N, West K W, Baldwin K W and Winkler R 2014 *Phys. Rev. Lett.* **112** 046804
[14] Peterson M R, Papić Z and Sarma S D 2010 *Phys. Rev. B* **82** 235312
[15] He S, Xie X C, Sarma S D and Zhang F C 1991 *Phys. Rev. B* **43** 9339

[16] Geraedts S, Zaletel M P, Papić Z and Mong R S 2015 *Phys. Rev. B* **91** 205139
[17] Fertig H 1989 *Phys. Rev. B* **40** 1087
[18] Tutuc E, Shayegan M and Huse D A 2004 *Phys. Rev. Lett.* **93** 036802
[19] Wen X G and Zee A 1992 *Phys. Rev. Lett.* **69** 1811
[20] Moon K, Mori H, Yang K, Girvin S M, MacDonald A H, Zheng L, Yoshioka D and Zhang S C 1995 *Phys. Rev. B* **51** 5138
[21] Girvin S M and MacDonald A H 1995 arXiv:cond-mat/9505087v1
[22] Kellogg M, Eisenstein J P, Pfeiffer L N and West K W 2004 *Phys. Rev. Lett.* **93** 036801
[23] Halperin B I 1983 *Hel. Phys. Acta* **56** 75
[24] Halperin B I, Lee P A and Read N 1993 *Phys. Rev. B* **47** 7312
[25] Shibata N and Yoshioka D 2006 *J. Phys. Soc. Jpn.* **75** 043712
[26] Zhu Z, Fu L and Sheng D N 2017 *Phys. Rev. Lett.* **119** 117601
[27] Sheng D N, Balents L and Wang Z Q 2003 *Phys. Rev. Lett.* **91** 116802
[28] Lian B and Zhang S C 2018 *Phys. Rev. Lett.* **120** 077601
[29] Eisenstein J P, Pfeiffer L N and West K W 2019 *Phys. Rev. Lett.* **123** 066802
[30] Liu X M, Li J I A, Watanabe K, Taniguchi T, Hone J, Halperin B I, Kim P and Dean C R 2022 *Science* **375** 205
[31] Moller G, Simon S H and Rezayi E H 2008 *Phys. Rev. Lett.* **101** 176803
[32] Isobe H and Fu L 2017 *Phys. Rev. Lett.* **118** 166401
[33] Wagner G, Nguyen D X, Simon S H and Halperin B I 2021 *Phys. Rev. Lett.* **127** 246803
[34] Scarola V W and Jain J K 2001 *Phys. Rev. B* **64** 085313
[35] Yoshioka D, Macdonald A H and Girvin S M 1989 *Phys. Rev. B* **39** 1932
[36] Read N and Green D 2000 *Phys. Rev. B* **61** 10267
[37] Zhu W, Liu Z, Haldane F D M and Sheng D N 2016 *Phys. Rev. B* **94** 245147
[38] Zhu Z, Sheng D N and Sodemann I 2020 *Phys. Rev. Lett.* **124** 097604
[39] Zhu Z, Sheng D N, Fu L and Sodemann I 2018 *Phys. Rev. B* **98** 155104
[40] Furukawa S and Ueda M 2012 *Phys. Rev. A* **86** 031604
[41] Wu Y H and Jain J K 2013 *Phys. Rev. B* **87** 245123
[42] Wu Y L, Regnault N and Bernevig B A 2013 *Phys. Rev. B* **110** 106802
[43] Sun K, Gu Z C, Katsura H and Sarma S D 2011 *Phys. Rev. Lett.* **106** 236803
[44] Ezawa Z F 2008 *Quantum Hall effects: Field theoretical approach, related topics*, 2nd Ed. (World Scientific Publishing Company)
[45] Willett R, Eisenstein J P, Stormer H L, Tsui D C, Gossard A C and English J H 1987 *Phys. Rev. Lett.* **59** 1776
[46] Pan W, Stormer H L, Tsui D C, Pfeiffer L N, Baldwin K W and West K W 2003 *Phys. Rev. Lett.* **90** 016801
[47] Mueed M A, Kamburov D, Pfeiffer L N, West K W, Baldwin K W and Shayegan M 2016 *Phys. Rev. Lett.* **117** 246801
[48] Zhang Y H, Mao D, Cao Y, Jarillo-Herrero P and Senthil T 2019 *Phys. Rev. B* **99** 075127
[49] Cao Y, Fatemi V, Fang S, *et al.* 2018 *Nature* **556** 43
[50] Cao Y, Fatemi V, Fang S, *et al.* 2018 *Nature* **556** 80
[51] Song J C W, Samutpraphoot P and Levitov L S 2015 *Proc. Acad. Natl. Sci. USA* **112** 10879
[52] Stefanidis N and Sodemann I 2020 *Phys. Rev. B* **102** 035158
[53] Liu J, Liu J and Dai X 2020 *Phys. Rev. B* **99** 155415
[54] Bernevig B A and Zhang S C 2006 *Phys. Rev. Lett.* **96** 106802
[55] Eugenio P and Dag C 2020 *SciPost Physics Core* **3** 015
[56] Zhang Y H 2018 arXiv:1810.03600 [cond-mat.str-el]
[57] Schleede J, Filinov A, Bonitz M and Fehske H 2012 *Contributions to Plasma Physics* **52** 819
[58] Boening J, Filinov A and Bonitz M 2011 *Phys. Rev. B* **84** 075130
[59] Astrakharchik G E, Kurbakov I L, Sychev D V, *et al.* 2021 *Phys. Rev. B* **103** L140101
[60] Shibata N and Yoshioka D 2004 *J. Phys. Soc. Jpn.* **73** 1
[61] Zhang Y H, Rezayi E H and Yang K 2014 *Phys. Rev. B* **90** 165102
[62] Rezayi E H, Haldane and Yang K 1999 *Phys. Rev. Lett.* **83** 1219
[63] Paquet D, Rice T M and Ueda K 1985 *Phys. Rev. B* **32** 5208
[64] Alicea J, Motrunich and Refael G F 2009 *Phys. Rev. Lett.* **103** 256403
[65] Anderson P W 1984 *Phys. Rev. B* **30** 1549
[66] Randeria M, Duan J M and Shieh L Y 1989 *Phys. Rev. Lett.* **62** 981
[67] Nozieres P and Schmitt-Rink S 1985 *J. Low Temp. Phys.* **59** 195
[68] Chin C, Bartenstein M, Altmeyer A, Riedl S, Jochim S, Hecker Denschlag J and Grimm R 2004 *Science* **305** 5687
[69] Greiner M, Regal C A and Jin D S 2003 *Nature* **426** 537
[70] Zwierlein M W 2014 *Superfluidity in ultracold atomic Fermi gases in Novel Superfluids* **2** 269
[71] Holland M, Kokkelmans, Chiofalo M L and Walser R 2001 *Phys. Rev. Lett.* **87** 120406
[72] Yang K and Zhai H 2008 *Phys. Rev. Lett.* **100** 030404
[73] Chen H and Yang K 2012 *Phys. Rev. B* **85** 195113